

https://doi.org/10.1070/QEL17291

Methods and algorithms for computer synthesis of holographic elements to obtain a complex impulse response of optical information processing systems based on modern spatial light modulators

E.Yu. Zlokazov

Abstract. **The possibilities of designing optical devices for data processing and imaging based on the manipulation of coherent light beams by means of spatial light modulators (SLMs) are investigated. A review of commercially available SLMs is presented and the limitations of their complex modulation characteristics are analysed. The main problem of using present-day SLMs is the lack of the ability to modulate directly all states within a unit circle in the complex plane. In this regard, the characteristics of current methods for the synthesis of holographic elements are described that implement a given complex impulse response of the optical system and are optimal for using SLMs with purely amplitude, purely phase, and hybrid amplitude–phase modulation.**

Keywords: *computer holographic synthesis, optical processing of information, spatial light modulators.*

1. Introduction

The use of the 2D distribution function of the complex amplitude of light as an information carrier is of great interest because it allows optical multichannel parallel transmission and processing of large arrays of digital data with speed and energy efficiency unattainable with pure electronics [1]. 2D and 3D imaging systems [2, 3], optical image encoding systems [4], coherent convolutional processors and correlators [5–10] are based on the principles of the formation of a complex impulse response of an optical system using 2D filtering masks. The spatial transmission function of the photomask, in the general case, is complex-valued. It is determined based on the parameters of the optical system in which the carrier light beam propagates, and with certain limitations can be found using the methods of the scalar diffraction theory [11]. Optoelectronic devices, such as a spatial light modulator (SLM) with high spatial resolution, allow fast introduction of filter elements into an optical system, which offers the prospects of developing dynamic devices for both imaging and real-time data processing.

The main problem when using present-day SLMs with high spatial resolution is that now there are no means for full-scale manipulation of the light complex amplitude. To solve this problem, the filtering photomasks displayed on the SLM screen must be somehow adapted to the characteristics of the device to ensure maximum signal-to-noise ratio at the output of the designed system.

In this regard, the main goal of this work is to assess the prospects of using commercially available SLMs for optical data processing and imaging based on the available types of light modulation and methods for synthesising holographic elements that implement a specified complex impulse response function of the optical system under conditions of a limited modulation characteristic of the used devices.

2. Optical system with a given complex impulse response

The formation of light signals with a given 2D distribution of complex amplitude is generally possible by realising a 2D filtering mask as a holographic element in a certain plane of the optical system. The transmission function of the mask is determined by the parameters of the generated signal and the configuration of the optical scheme of light beam propagation from the plane of filtration to the plane of the observed output signal. The use of a Fourier-transforming lens (FTL) and a Fourier-reconstructing lens (FRL) in the 4*f* configuration allows applying spatial-frequency filtering methods to processing and generating light signals with a given spatial distribution of complex amplitude.

Figure 1 shows a typical 4*f* scheme with a Fourier filter in the spatial frequency plane. The front focal plane of the FTL with focal length f_1, represented in Cartesian coordinates x_1, y_1, is called the input image plane with the distribution function of the complex amplitude $a(x_1, y_1)$. In this plane, the input signal of the optical system forms. The transparency filter with the 2D distribution function of the transmittance $T(u, v)$ is located in the rear focal plane of the FTL, which is also the front focal plane of the FRL. In Fig. 1, this plane is character-

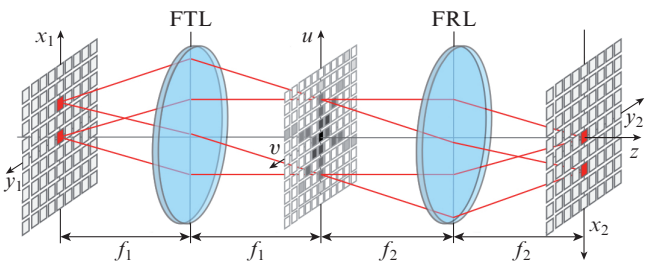

Figure 1. Schematic of a 4*f* coherent convolutional processor.

E.Yu. Zlokazov National Research Nuclear University MEPhI, Kashirskoe sh. 31, 115409 Moscow, Russia;
e-mail: ezlokazov@gmail.com

Received 18 February 2020; revision received 13 March 2020
Kvantovaya Elektronika **50** (7) 643–652 (2020)
Translated by V.L. Derbov

ised by Cartesian coordinates u,v. The rear focal plane of the FRL with the focal length f_2 is characterised by the Cartesian coordinates x_2, y_2 and is referred to as the output image plane.

If $x_2 = -x_1 f_2/f_1$, $y_2 = -y_1 f_2/f_1$, $u = x_1/(\lambda f_1)$, and $v = y_1/(\lambda f_1)$, (λ being the radiation wavelength), then the distribution function of the complex light amplitude in the output image plane can be related to that in the input image plane as [11]

$$f(x_2, y_2) = \mathcal{F}^{-1}[A(u,v)T(u,v)](x_2, y_2) = \langle a \odot t \rangle (x_2, y_2), \quad (1)$$

where $A(u,v) = \mathcal{F}[a(x_1, y_1)](u,v)$ is the Fourier transform of the function $a(x_1, y_1)$ in the spatial coordinates u,v; $\langle a \odot t \rangle (x,y)$ denotes the convolution of the functions a and t in the coordinates x, y. If we place a point source of monochromatic radiation in the centre of the $(x_1 y_1)$ plane, then $A(u,v) = \text{const}$, and the distribution function of the complex amplitude in the output plane of the system will be proportional to the inverse Fourier transform of the function T:

$$f(x_2, y_2) \propto t(x_2, y_2) = \mathcal{F}^{-1}[T(u,v)](x_2, y_2). \quad (2)$$

This configuration underlies coherent imaging systems using Fourier holograms. In the present case, the function $T(u,v)$ is calculated such that its inverse Fourier transform, the function $t(x_2, y_2)$, contains the desired image.

The possibility of analogue implementation of the convolution of two functions in an optoelectronic coherent processor can be used to solve a wide range of problems, such as filtering and correlation recognition of images [12], ghost imaging [13], implementation of multi-channel parallel computations in partial derivatives [14, 15], as well as the modelling of optical neural networks [16]. When designing a coherent 4*f* scheme for correlation recognition problems, in the $(x_1 y_1)$-plane an image of a scene is formed containing images of objects to be recognised, and the Fourier filter $T(u,v)$ implements an impulse response corresponding to the reference pattern presented in the object plane as a function $t(x,y)$. In the $(x_2 y_2)$ plane, an image of the correlation function of the input scene with the reference function is formed.

In the simplest case of a matched filter,

$$T(u,v) = A^*(u,v), \quad (3)$$

expression (1) becomes identical to the formula for autocorrelation, and the output signal is a bright and narrow correlation peak. A well-known problem of matched filtering is high sensitivity to noise and image distortion of a recognised object relative to the reference one. Therefore, composite invariant filters synthesised in the form of a linear or nonlinear combination of a set of training images that allow achieving the stability of correlation recognition in the presence of distortions, such as rotation, scaling, partial overlap, changes in illumination, etc., are now widely used [12, 17, 18].

Thus, in the general case in order to generate the required signal in the output plane of the optical system shown in Fig. 1, the function representing the 2D transmission of the Fourier filter $T(u,v)$ should be complex.

3. Commercially available SLMs

The use of electronically controlled SLMs allows the processing of optical signals and the formation of images in real time. The operation speed of such systems is largely determined by the number of active elements in the discrete structure of the SLM screen and the speed of their switching; therefore, spatial resolution, type of modulation, and frame rate are deci-

Table 1. Commercially available SLMs with high spatial resolution.

Model	Manufacturer	Technology	Resolution	d_0 /μm	ν /Hz
LCX202A	Sony	TLC	1924 × 1024	7.2	240
SXRD241A	Sony	LCOS	1920 × 1080	4.25	60
4K	Compound Photonics	LCOS	4096 × 2160	3.015	120
HX7318	Himax	LCOS	1366 × 768	6.0	360
D-ILA	JVC	LCOS	4096 × 2400	6.8	220
LC-2012	Holoeye	TLC	1024 × 768	32	60
GAEA-2	Holoeye	LCOS	4160 × 2464	3.74	60
LETO	Holoeye	LCOS	1080 × 1920	6.4	60/180
X13138	Hamamatsu	LCOS	1272 × 1024	12.5	60/120
OP02220	OmniVision	LCOS	1280 × 720	4.5	300
RDP700Q	RaonTech	LCOS	2560 × 1440	6.05	360
SLM-200	Santec	LCOS	1200 × 1920	8.0	60/120
SYL2341	Syndiant	LCOS	3840 × 2160	3.2	60
HSP1920	Meadowlark Optics	LCOS	1920 × 1152	9.2	30–422
JD4704	Jasper	LCOS	4160 × 2464	3.74	180
QXGA	ForthDD	FLCOS	2048 × 1536	8.2	5700
UXGA	MDCA	FLCOS	1600 × 1200	6.3	540
DLP7000	Texas Instruments	DMD	768 × 1024	13.6	32552
DLP9500	Texas Instruments	DMD	1080 × 1920	10.8	23148
1M SLM	Fraunhofer IPMS	AMM	2048 × 512	16	2000
1D LM	Fraunhofer IPMS	AMM	8000 × 1	10	1 MHz
G8192	Silicon Light Machines	GLV	8192 × 1	5	250 kHz

Note: d_0 is the pixel size and ν is the frame rate.

sive in the design of an optical information processing and imaging system.

Table 1 provides an overview of commercially available (at the time of writing) spatial light modulation devices having high spatial resolution (more than ~1 megapixel), as well as a frame rate of about 60 Hz or more. As a result, we can conclude that today only two types of devices are available that meet the required characteristics, namely, SLMs whose principle of operation is based on the use of liquid crystals (LC), and microelectromechanical systems (MEMS).

In the case of LC SLMs, two different manufacturing technologies can be distinguished, using transmissive liquid crystal (TLC) and reflective liquid crystal on silicon (LCOS) structures. Also worth highlighting, is the group of liquid-crystal SLMs based on ferroelectric LC (FLCOS), which have the highest frame rate among all LC-based devices, as well as some unique modulation properties. MEMSs are represented by two fundamentally different types: systems based on a micromirror matrix, such as DMD^{TM} (digital micromirror device [19]) and AMM (active micromirror matrix), and systems based on grating light valve (GLV^{TM}) [20, 21]. Many of these devices have specific features that must be considered when designing an optical system. Thus, the specific features of Hamamatsu (X13138) liquid crystal SLMs are linear phase characteristic, high accuracy of phase control, and high light efficiency for specific wavelengths due to the use of a dielectric mirror. The Santec (SLM-200) devices possess high flatness (up to $\lambda/40$), as well as high input signal resolution of 10 bits, which makes it possible to carry out high-precision control of the beam phase. The Meadowlark Optics (HSP1920) device is controlled by an analogue driver, which allows increasing the frame rate to 422 Hz. The Syndiant (SYL2341) devices have the smallest minimum pixel size, they are the most compact and, therefore, in demand for head-mounted displays.

The frame rate of all types of MEMS-based SLMs ranges from 10 kHz to 1 MHz, which is especially attractive for the development of high-transfer-rate optical digital devices. However, it is important to keep in mind that devices of the DMD^{TM} and AMM types have a fundamentally binary amplitude modulation characteristic, and GLV^{TM}-based devices, as a rule, have high resolution in only one spatial coordinate, so that for operating in 2D mode in an optical scheme temporal scanning in low-resolution coordinate is necessary. The frame rate ~1 MHz of the 1D LM device (Fraunhofer IPMS) allows achieving a frame rate up to 500 Hz for a 2D function consisting of 2000 lines, which is comparable to the frame rate for the best LCD-based SLMs, and the resolution of 8000 pixels per line makes possible imaging with record-breaking spatial resolution.

Figure 2a shows a phasor diagram of a typical complex Fourier filter. Figures 2b–2h present typical diagrams of the available modulation states that are potentially achievable using the devices summarised in Table 1.

Continuous amplitude modulation (Fig. 2b) is available using LC-based SLMs [22], as well as MEMS modulators of the GLV^{TM} type. However, when implementing a Fourier filter, it should be borne in mind that for some types of liquid-crystal SLMs, the operation in the amplitude mode can be accompanied by additive phase modulation, so that the modulation characteristic may look similar to that shown in Fig. 2c. This can lead to errors and distortions at the output of the designed optical system [23, 24]. A special case of amplitude modulation, the binary amplitude modulation (Fig. 2d),

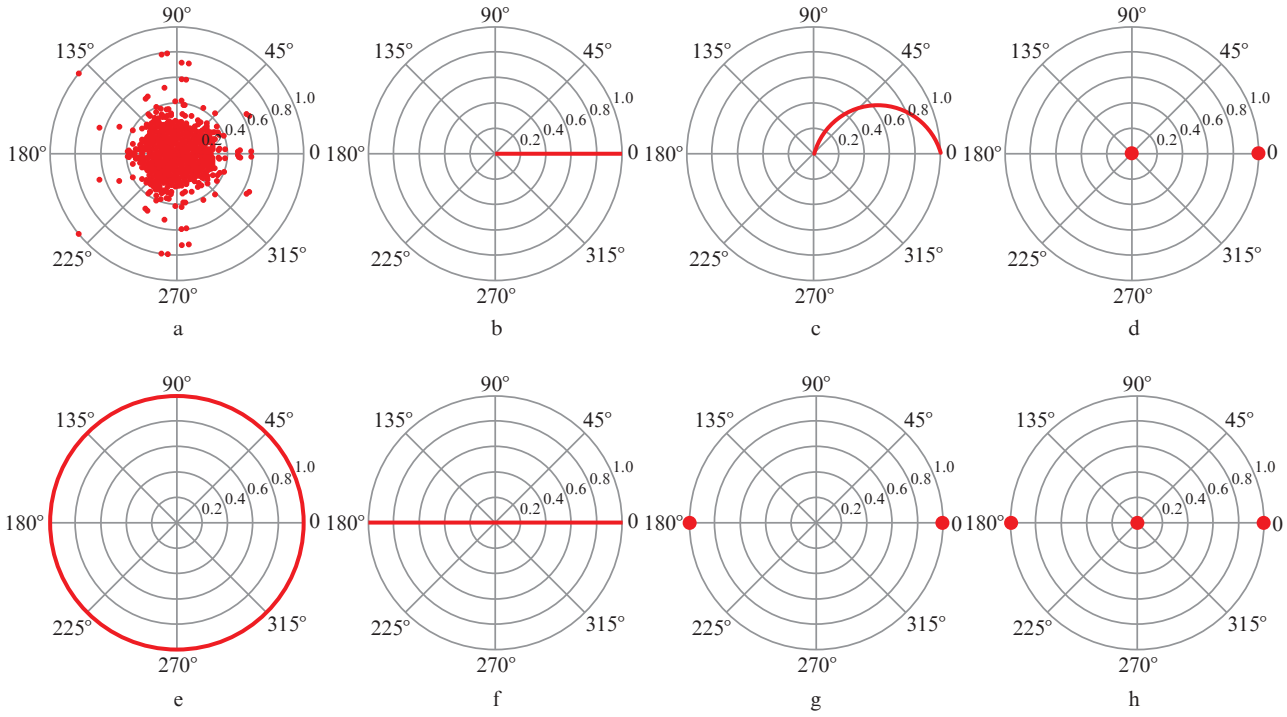

Figure 2. Representation of states with different types of modulation available using modern SLMs on the unit circle in a complex plane: (a) example of a phase diagram of a complex Fourier filter; (b) pure amplitude modulation; (c) amplitude modulation with additive phase shift; (d) binary amplitude modulation; (e) pure phase modulation; (f) bipolar amplitude modulation; (g) binary phase modulation; (h) ternary amplitude modulation.

is implemented using FLCOS-based SLMs, as well as MEMS based on an active micromirror matrix (DMD^{TM} and AMM). Pure phase modulation is possible using most LC-based SLMs [22], as well as GLV^{TM}-based MEMS SLMs. The combination of binary phase and continuous amplitude modulations, i.e., bipolar continuous amplitude modulation (Fig. 2f), can be obtained using SLMs based on nematic LCs with zero twist [25, 26] or ferroelectric LCs [22]. Binary phase (Fig. 2g) and ternary bipolar amplitude (Fig. 2f) modulation characteristics can be obtained using some types of SLMs based on both nematic twist structures [27, 28] and ferroelectric LC [22].

In the present work, the quantised or binary types of modulation characteristics presented in Figs 2d, 2g, and 2h are considered as special cases of a continuous unipolar or bipolar modulation characteristic. Methods such as binarisation and rasterisation are used to suppress distortion caused by limiting the number of quantisation levels. A detailed discussion of these issues is beyond the scope of this article. The results of studies on the use of binary SLMs in free-space optical systems are given in Ref. [29].

Thus, at the moment there is no SLM, the unit cells of which are capable of carrying out full-fledged complex modulation of light for all states on a unit circle in the complex plane. Available types of modulation characteristics can be divided into three main groups: purely amplitude, purely phase, and combined amplitude–phase (amplitude with additive phase shift and bipolar amplitude) modulations.

One approach to implementing the complex response function is to use optical schemes based on two SLMs [30–33], as well as schemes using different zones of the SLM to form beams, the interference of which generates the desired function [34]. However, as a rule, these schemes are very complicated and therefore their detailed consideration is beyond the scope of this work. Of particular interest is the approach consisting in the use of the synthesised holographic filter $\Gamma(u,v)$ instead of the transparency $T(u,v)$. Below we present methods for implementing the impulse response of a coherent optical system based on using only one SLM in the optical scheme.

4. Methods of forming a complex impulse response using amplitude SLMs

An early attempt to implement a holographic Fourier filter using a purely amplitude binary mask was the detour phase method described in the classical works of Brown and Lohmann [35, 36] and Lohmann and Paris [37, 38]. The idea of the method is to represent the discrete complex element of the Fourier filter in the form of a rectangular slit, the area of which is proportional to the amplitude, and the displacement of the slit within the element aperture is proportional to the phase of the corresponding element of the Fourier filter. The practical application of this method using SLM with a prespecified discrete structure of elements would require a significant margin of resolution, because for each discrete filter element, a large number of SLM pixels would have to be used. In this case, the modulation characteristic would take strictly defined discrete values in amplitude and phase. Below we consider methods that do not require significant redundancy in the resolution of SLM for their physical implementation.

4.1. Macropixel method

The macropixel method consists in encoding discrete values of the Fourier filter complex amplitude using several SLM elements. Lee [39] was the first to propose using four pixels of an amplitude SLM to represent values of an arbitrary complex function. According to the Lee method, a complex impulse response in the object plane $f(x,y)$ is formed by placing the amplitude hologram $\Gamma(u,v)$ in the plane of Fourier frequencies of the optical system. To find the holographic filter function, the complex amplitude of the impulse response Fourier transform can be represented as the sum of two pairs of mutually compensating vectors:

$$|F(u,v)|\exp[\mathrm{i}\Phi(u,v)] = F_1(u,v) - F_3(u,v) + \mathrm{i}F_2(u,v) - \mathrm{i}F_4(u,v), \tag{4}$$

where $F(u,v)$ is the real amplitude and $\Phi(u,v)$ is the real phase of the Fourier transform of the function $f(x,y)$. Non-negative real functions of the kth subpixel $F_k(u,v)$ can be determined by the formulas

$$\begin{aligned} F_1(u,v) &= \begin{cases} |F(u,v)|\cos\Phi(u,v), & \cos\Phi(u,v) > 0, \\ 0, & \cos\Phi(u,v) \leqslant 0, \end{cases} \\ F_3(u,v) &= F_1(u,v) - |F(u,v)|\cos\Phi(u,v), \\ F_2(u,v) &= \begin{cases} |F(u,v)|\sin\Phi(u,v), & \sin\Phi(u,v) > 0, \\ 0, & \sin\Phi(u,v) \leqslant 0, \end{cases} \\ F_4(u,v) &= F_2(u,v) - |F(u,v)|\sin\Phi(u,v). \end{aligned} \tag{5}$$

Then the discrete real non-negative transmission function of the amplitude hologram can be represented as

$$\Gamma(u,v) = \sum_{m=-\infty}^{\infty}\sum_{n=-\infty}^{\infty}\sum_{k=1}^{4} F_k(u,v)\,\delta\left(u - \frac{n}{N} + \frac{k-1}{4N}, v - \frac{m}{M}\right), \tag{6}$$

where $N \times M$ is the physical size of the discrete holographic filter. It is important to note that subpixels are arranged along one of the spatial discretisation directions having a dimension of N elements. The actual dimension of the implemented complex Fourier filter is $(N/4) \times M$. The response of such a filter can be found by calculating the inverse Fourier transform of function (6):

$$\begin{aligned} \gamma(x,y) &= \sum_{m=-\infty}^{\infty}\sum_{n=-\infty}^{\infty}\sum_{k=1}^{4} f_k(x - mM, y - nN)\exp\left[\frac{\mathrm{i}n(k-1)\pi}{2}\right] \\ &= \sum_{m=-\infty}^{\infty}\sum_{n=-\infty}^{\infty} t_n(x - mM, y - nN), \end{aligned} \tag{7}$$

where $f_k(x,y)$ is the Fourier transform of the function $F_k(u,v)$;

$$t_n(x,y) = \sum_{k=1}^{4} f_k(x - mM, y - nN)\exp\left[\frac{\mathrm{i}n(k-1)\pi}{2}\right]. \tag{8}$$

In Eqn (8), the term $t_1(x,y)$ is the inverse Fourier transform of the complex function represented by Eqn (4), whence it can be concluded that $t_1(x,y) = f(x,y)$. Thus, it is possible to

find a purely amplitude filter that forms in the object plane an image of the desired impulse response $f(x,y)$.

The Lee method was further developed in Ref. [40], where, based on a similar idea, it was possible to realise the complex function of the Fourier filter with the help of macropixels consisting of three amplitude SLM subpixels. The key idea is to represent the Fourier transform of the function $f(x,y)$ as the sum of three terms:

$$|F(u,v)|\exp[i\Phi(u,v)] = F_1(u,v) + F_2(u,v)\exp(i2\pi/3) + F_3(u,v)\exp(i4\pi/3). \quad (9)$$

Here the non-negative real-valued functions of the kth subpixel $F_k(u,v)$ are given in the form

$$F_1(u,v) = \begin{cases} |F(u,v)|\cos\Phi + 3^{-1/2}\times \\ \times|F(u,v)|\sin\Phi, & 0 \leqslant \Phi \leqslant 2\pi/3, \\ 0, & 2\pi/3 \leqslant \Phi \leqslant 4\pi/3, \\ 3^{-1/2}|F(u,v)|\sin\Phi'', & 4\pi/3 \leqslant \Phi \leqslant 2\pi, \end{cases}$$

$$F_2(u,v) = \begin{cases} 3^{-1/2}|F(u,v)|\sin\Phi, & 0 \leqslant \Phi \leqslant 2\pi/3, \\ |F(u,v)|\cos\Phi' + 3^{-1/2}\times \\ \times|F(u,v)|\sin\Phi', & 2\pi/3 \leqslant \Phi \leqslant 4\pi/3, \\ 0, & 4\pi/3 \leqslant \Phi \leqslant 2\pi, \end{cases} \quad (10)$$

$$F_3(u,v) = \begin{cases} 0, & 0 \leqslant \Phi \leqslant 2\pi/3, \\ 3^{-1/2}|F(u,v)|\sin\Phi', & 2\pi/3 \leqslant \Phi \leqslant 4\pi/3, \\ |F(u,v)|\cos\Phi'' + 3^{-1/2}\times \\ \times|F(u,v)|\sin\Phi'', & 4\pi/3 \leqslant \Phi \leqslant 2\pi, \end{cases}$$

where $\Phi' = \Phi - 2\pi/3$; $\Phi'' = \Phi - 4\pi/3$. Then the discrete function for calculating the amplitude hologram in the Fourier plane of the system can be written in the form

$$\Gamma(u,v) = \sum_{m=-\infty}^{\infty}\sum_{n=-\infty}^{\infty}\sum_{k=1}^{3} F_k(u,v) \times \delta\left(u - \frac{n}{N} + \frac{k-1}{3N}, v - \frac{m}{M}\right). \quad (11)$$

It is important to note that in this case, 25% of the spatial resolution of the filter is saved compared to the original Lee method.

The disadvantage of the described multipixel methods is that due to the purely amplitude implementation of the filter in the plane of the Fourier frequencies, a bright zeroth order and conjugate image will always be observed in the image plane. In order to prevent the response image from overlapping with the zeroth order and the conjugate image, an additional phase slope is added to the Fourier filter function, similar to the off-axis hologram method discussed below in Section 4.2. The maximum value of this slope is limited by the resolution of the SLM. Thus, the resolution of the implemented Fourier filter will not exceed 1/8 of the SLM resolution in the case of the four-pixel Lee method, and 1/6 in the case of the three-pixel version.

In the presented methods of the macropixel approach, spatial-frequency filtering of the image is necessary using the spatial Nyquist filter, the width of which is determined by the quantity $\Delta u = \lambda f/(ld_0)$ in one of the coordinates and $\Delta v = \lambda f/d_0$ in the other coordinate. Here l is the number of subpixels in one macropixel, d_0 is the pixel size, and f is the focal length of the FRL.

4.2. Synthesis of an off-axis amplitude hologram

The holographic method for recording complex light fields is based on adding a reference beam to the object beam, which carries information about the complex amplitude of the recorded field, with the aim of forming an interference field to be recorded with a photosensitive carrier [41]. The resulting hologram is an amplitude fringe pattern. If such a pattern is illuminated with a reference beam, the image of the recorded object will be restored in the appropriate plane of the system. Using numerical models of the reference and object beams in the plane of the holographic carrier, we can calculate the spatial distribution of the interference pattern in the form of a discrete array of real values. Figure 3 shows the scheme of recording an amplitude Fourier hologram and subsequent image formation with a reference beam (dash-dotted lines) formed by a point radiation source $o(x,y)$ located in the front focus of the FTL. The object beam (dashed lines) is formed by the scattering object $a(x,y)$, separated from the reference point source by a distance Δ_x along the x axis.

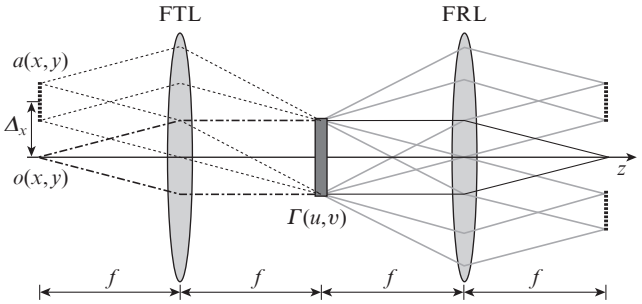

Figure 3. Scheme for recording and reading an amplitude Fourier hologram.

A thin layer of the photosensitive material of the plate located in the back focal plane of the FTL will record the intensity of the interference pattern of the object and reference beams in the form of a 2D structure with a distribution of transmittance values:

$$\Gamma(u,v) \propto |A_r(u,v) + A_d(u,v)|^2 = |A_r|^2 + |A_d|^2 + A_r^* A_d + A_r A_d^*, \quad (12)$$

where $A_r(u,v) = \text{const}$ is the amplitude of the reference beam; and $A_d(u,v)$ is the complex amplitude of the object beam, which can be represented as

$$A_d(u,v) = \mathcal{F}[a(x,y)](u,v)\exp(-i2\pi\Delta_x u).$$

In the numerical synthesis of the holographic element, the cross-correlation terms in formula (12) can be excluded, since they do not contain information useful for reconstructing the image of an object, and, in addition, they are sources of parasitic interference. Then the basic equation for calculating the

pattern of a computer-generated Fourier hologram (CGFH) can be simplified in the form

$$\Gamma(u,v) = \mathrm{Re}\{\mathcal{F}[a(x,y)](u,v)\exp(-\mathrm{i}2\pi\Delta_x u)\}. \quad (13)$$

The function $\Gamma(x,y)$ takes only real values and can be directly implemented using SLMs with bipolar amplitude modulation (Fig. 2f). For its implementation using SLMs with unipolar amplitude modulation (Fig. 2b), the amplitude shift must be added to the function $\Gamma(x,y)$:

$$\Gamma'(u,v) = \Gamma(u,v) + C, \quad (14)$$

where

$$C \geqslant -\min_{u,v}\Gamma(u,v). \quad (15)$$

The resolution of the SLM used to implement the CGFH function $\Gamma'(u,v)$, as well as the presence of a conjugate image, limit the resolution of the object being realized to $(N/2) \times M$, where N and M are the numbers of discrete SLM elements along the axes u and v, respectively [42].

The method based on the synthesis of amplitude holographic patterns is most often used when implementing complex Fourier filters in coherent 4*f* image correlators [43–48]. Illustrative examples of the application of the high-resolution imaging scheme based on the CGFH are the archive holographic memory system [49, 50] and the symbolic information output device in the augmented reality system [51], developed and studied at the Bauman Moscow State Technical University.

5. Methods for the formation of a complex impulse response using purely phase SLMs

A number of authors have shown that in the simplest case, only the phase component of the Fourier filter function in the plane of the Fourier frequencies of the system can be used. An example of possible application of this approach is the implementation of correlation filters in a coherent 4*f* correlator [52, 53]. However, it must be understood that with such an implementation, part of the useful information is lost and the brightness of minor elements of the generated response increases, which does not guarantee the correctness of the output signal in all possible situations of the designed optical system functioning. In the case of using an imaging system, equating the amplitude component of the Fourier filter elements to the same value will lead to distortions of the generated scene, consisting, e.g., in enhancing the brightness of sharp-gradient areas and contours.

5.1. Synthesis of kinoform

In some cases, phase information is not important and it is necessary to restore only the intensity of the light distribution, but the high diffraction efficiency of the optical system is important. Examples of such optical devices are coherent imaging systems for visual observation. In such cases, a method of synthesising purely phase holograms can be used. In accordance with this method, the image of the object is first encoded with a random phase mask, while the density of the spatial frequency spectrum is significantly increased and the amplitude of the zeroth order decreases. Next, a complex impulse response is calculated. For the physical realisation, only the phase of such a synthesised hologram is used. In order to improve the quality of the reconstructed image, iterative synthesis algorithms are used.

The iterative Gerchberg–Saxton algorithm (GSA) [54], as well as its modifications [55–58], are the most efficient and frequently used methods for the synthesis of phase kinoforms of various types. The basic flow diagram of the GSA is shown in Fig. 4. First, a random phase mask φ_0 is added to the amplitude a_0 of the digital image of the holographic object. Next, the iterative algorithm itself is launched, which consists in calculating the inverse integral optical conversion (IIOC) of the complex amplitude from the object plane to the kinoform plane (steps 1 and 2), unifying the obtained amplitude factor A_n (n being the iteration number) of the kinoform (step 3), and calculating the direct integral optical conversion (IOC, step 4), as well as in the analysis of the amplitude of the reconstructed image and verification of the fulfillment of the condition for exiting the loop. As a criterion for exiting the loop, e.g., the standard deviation $\sigma(a_n, a_0)$ of the amplitude of the image a_n obtained in step 4 from the amplitude of the original holographic image a_0 is used. If the condition for exiting the loop is not fulfilled, the next iteration is started, and in step 1, a new complex image function with the amplitude a_0 and phase φ_n obtained in step 4 of the previous iteration is formed. If the condition for exiting the loop is fulfilled, the result of the algorithm execution is the function of the kinoform phase argument Φ_n, obtained in step 2. Depending on the application conditions of the synthesised kinoform, the appropriate integral transformation is selected: Rayleigh–Sommerfeld or its Fresnel or Fraunhofer approximations, as well as analogues of these approximations underlying the method of angular spectrum propagation [11].

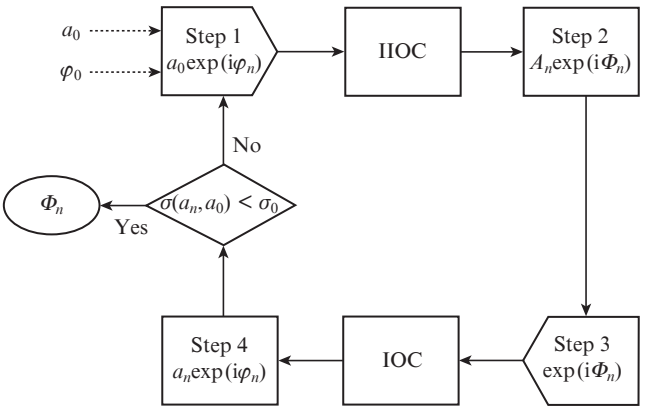

Figure 4. GSA flow diagram.

The obvious drawback of iterative synthesis algorithms is the large time expenditure, as well as the impossibility of generating a wave with simultaneously specified values of the amplitude and phase. Therefore, this approach has limited application to problems where fast recalculation or correction of the complex impulse response is required.

5.2. Realisation of synthesised patterns of amplitude holograms using purely phase SLMs

Transferring the amplitude pattern of a Fourier hologram into pure phase (bleaching) is a well-known method for obtaining holograms with high diffraction efficiency. Similarly, it is possible to realise the amplitude patterns of Fourier holograms synthesised in accordance with formula (13) by displaying them on a pure phase SLM:

$$\Gamma_{\text{ph}}(u,v) = \exp\left[\text{i}\frac{\alpha}{\max\Gamma(u,v)}\Gamma(u,v)\right], \tag{16}$$

where α is the coefficient (in rad), which has the meaning of the phase modulation depth.

An important problem in this case is the presence of higher diffraction orders in the holographic pattern in the output light field of the optical system. Thus, it was shown in [59] that if a Fourier hologram is used to form a high-resolution image (an image of a binary data page of archive holographic memory), the presence of higher harmonics during phase modulation leads to a significant decrease in the signal-to-noise ratio of the reconstructed amplitude–phase image data pages with a phase modulation depth greater than $\pi/2$. In this case, the diffraction efficiency for the depth of phase modulation $\pi/2$ turns out to be comparable with the diffraction efficiency of a purely amplitude hologram. Thus, the method of synthesising CGFHs and its implementation using phase-modulating carriers has a number of limitations when solving high-resolution imaging problems, especially when exact reconstruction of the complex values of the spatial distribution function of the light beam amplitude is required.

When developing a coherent system of correlation recognition, the output useful signal is the image of the area of the cross-correlation peak, which occupies a small area of the output light field. The presence of spatial harmonic interference arising from the implementation of the GGSF of the synthesised invariant filter using a phase SLM does not actually affect the signal-to-noise ratio of the detected correlation signal. In Ref. [60], using an example of the implementation of an invariant MINACE filter, it was shown that within a phase modulation depth range $\pi-4\pi$ an increase in the diffraction efficiency of the holographic filter improves the discriminatory characteristic of the recognition system compared to the purely amplitude implementation described in Section 4.2 of this paper. The minimum error estimated by the Neyman–Pearson criterion was observed at a modulation depth of $\sim 2\pi$ and amounted to 2.9%, which turned out to be 0.7% less than for a purely amplitude implementation of a holographic filter.

5.3. Double-phase coding method

In Refs [61–63], the possibility of complete complex modulation using a purely phase SLM was shown. In this case, a macropixel is represented by two subpixels of a SLM. An arbitrary complex number $a(x,y)$ can be represented on the unit circle in a complex plane as the sum of two phasors with the same amplitude:

$$a(x,y) = |a|\exp(\text{i}\varphi) = \frac{1}{2}[\exp(\text{i}\theta_1) + \exp(\text{i}\theta_2)], \tag{17}$$

where θ_1 and θ_2 are the phase shifts of the first and second subpixels of the common macro-pixel. It can be seen from Fig. 5 that by choosing the values of θ_1 and θ_2, one can obtain any complex number from the unit circle. This method is also known as the double-phase coding method. The values of subpixels can be found, for example, in the form [61]

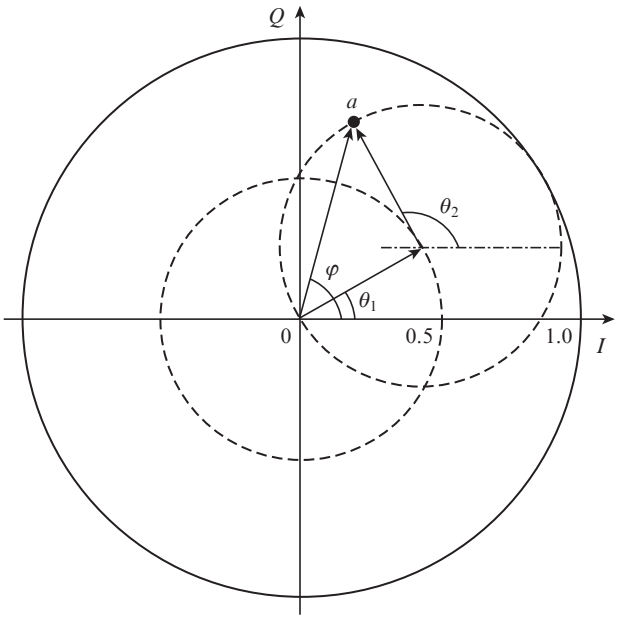

Figure 5. Presentation diagram of an arbitrary complex number on a unit circle using two phase-modulating SLM elements.

$$\theta_1 = \varphi + \Delta\varphi, \quad \theta_2 = \varphi - \Delta\varphi, \tag{18}$$

where

$$\Delta\varphi = \arccos\frac{|a|}{2}. \tag{19}$$

It is worth noting that representation (17) of a complex number as a sum of two complex numbers with the same real amplitude was also used in a scheme, in which a complex impulse response is formed due to the double passage of the reading beam through different regions of the same phase modulator [34]. Dividing the total beam in the Fourier plane into two beams and the appropriate phase manipulations in each channel made it possible to compensate for the spatial phase shift in the object plane between these regions and to obtain the corresponding sum from Eqn (17).

6. Methods for the formation of a complex impulse response using SLMs with combined types of amplitude–phase modulation

Theoretical studies [23, 24] and [59] showed that the presence of additive phase modulation can significantly reduce the signal-to-noise ratio of the output optical signal both for optical correlation problems and for complex imaging systems [59]. An accurate measurement of the modulation characteristic will allow optimisation of the output filter function and compensation of the resulting distortions [23, 24]. This section discusses some approaches to implementing a complex Fourier filter using devices with combined amplitude-phase mod-

ulation, such as additive hybrid and bipolar amplitude modulation.

6.1. Optimal projection method

In some cases the complex impulse response of a coherent 4*f* correlator can be realised with SLMs having a limited number of hybrid amplitude and phase modulated states on a unit circle in the complex plane by searching for the optimal projection of the Fourier filter complex function on the space of available states of the modulation characteristic [64–66]. The idea of this approach is to find the projection of the Fourier filter complex function on the modulation characteristic of the SLM, for which the optimisation objective function will be minimal. As optimisation functions, one can use general metrics, such as the L^p norm, in particular, the Euclidean distance L^2, as well as metrics specific to correlation recognition. Examples of the latter are the ratio of the autocorrelation peak intensity to the total correlation field energy (peak-to-correlation ratio, PCR) and the ratio of the peak intensity to the mean energy in the surrounding region (peak-to-sidelobe ratio, PSR). As parameters for choosing the filter projection to represent the set of its values, the scaling coefficient μ and the rotation parameter ϕ of the set of filter values in the phasor diagram can be used. The optimisation problem of finding the projection of the Fourier filter values onto the set of available SLM states can be described by the expression

$$\Gamma_{\text{opt}} = \underset{\Gamma_{\mu\phi} \in \mathcal{D}^N}{\operatorname{argmin}} \left[\sum_{k=0}^{N-1} \left| (\Gamma_{\mu\phi})_k - (\mu \Gamma_0 \exp(\mathrm{i}\phi))_k \right|^2 \right], \tag{20}$$

where Γ_0 is the N-dimensional function of the initial Fourier filter; Γ_{opt} is the desired optimal function for representing the holographic filter using SLM; and the argument $\Gamma_{\mu\phi}$ is the Euclidean projection of the scaled and rotated filter $\mu\Gamma_0 \exp(\mathrm{i}\phi)$ onto the surface of possible states of the SLM transmission function represented by the set $\mathcal{D}^N$.

In Ref. [49], the problem of implementing Fourier filters in a 4*f* correlator of images using SLMs having a spiral, binary amplitude or binary phase modulation characteristic (see Figs 2c, 2d, and 2g) was investigated. It is worth of particular note, that one of the research results presented in [49] is a decrease in the error probability of recognition system when using the synthesised projection of the Fourier filter on the space of SLM values in the case of a spiral hybrid characteristic of SLM as compared to the system based on the initial complex Fourier filter.

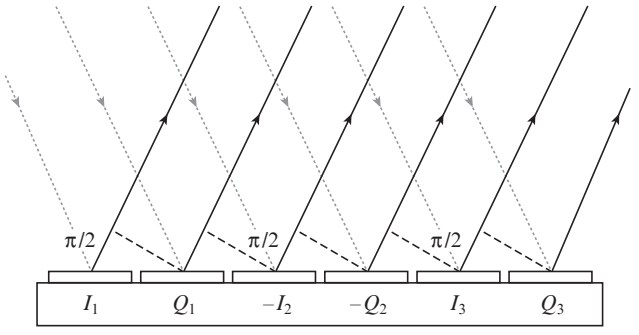

Figure 6. Configuration of SLM elements with bipolar amplitude modulation for the implementation of a complex filter by the two-element quadrature macropixel method.

6.2. Quadrature macropixel method

This method is based on the use of reflective SLMs with bipolar amplitude modulation. This method was implemented using SLMs with a nematic LC with zero twist [26] and SLMs with a ferroelectric LC [67–69]. The essence of the method is the quadrature representation of a complex number in the form of the sum

$$A(u,v) = I(u,v) + \mathrm{i}Q(u,v), \tag{21}$$

where $I(u,v)$ and $Q(u,v)$ are the real amplitudes of the in-phase and quadrature components of the signal, respectively. Two adjacent SLM subpixels belonging to one macro-pixel modulate in-phase and quadrature amplitudes. The shift by π/2 between the subpixels is achieved due to the configuration of the optical illumination scheme of the SLM, in which the phase shift between adjacent pixels having the same value is π/2. In this case, the amplitudes for each second macro-pixel are taken with the opposite sign (Fig. 6).

The quadrature pixel method was successfully demonstrated in the implementation of the holographic imaging system [67] and was used in the 4*f* image correlator scheme [68].

The idea of the optical configuration of the read beam and the SLM with a quadrature phase shift between adjacent pixels in one of the spatial directions was generalised to the version with an arbitrary modulation characteristic of the SLM. The method was demonstrated using a liquid crystal SLM with a nematic twist structure possessing a hybrid amplitude-phase modulation [70], similar to that shown in Fig. 2c.

7. Conclusions

The advantages and disadvantages of the basic methods for the formation of a 2D complex pulse response of an optical system using commercially available spatial light modulation devices with high spatial resolution are considered. A review of the available SLMs showed that modern fast operating devices have a spatial resolution of up to 10 megapixels, but there are currently no means for direct control of the amplitude and phase of the beam. The main types of modulation available are purely amplitude, purely phase, and hybrid amplitude–phase modulation. To synthesise the holographic element structure that implements a given complex impulse response using a device with a purely amplitude modulation characteristic, the Lee macropixel method and its improved versions, the quadrature multipixel method, as well as the method of synthesis of an amplitude off-axis Fourier hologram (CGFH) can be used. The latter is the most promising for use, because it allows the high-precision formation of a complex impulse response with only two-fold redundancy of the resolution of the SLM.

In the case of a purely phase modulation characteristic of the SLM, the kinoform synthesis method, the paraphase encoding method, and the method based on the amplitude CGFH structures for modulating the phase shift can be used to form a complex impulse response. The disadvantage of the kinoform iterative method is the large computing expenditures in the synthesis. The paraphase encoding method, as well

as the CGFH-based method, allow implementation of the complex impulse response function with twice the redundancy of the SLM resolution. When using the CGFH amplitude structures to modulate the phase shift, the presence of higher orders can limit the accuracy of the designed system, especially if the system is used to restore images with high spatial resolution. However, if the output signal is the correlation function of the input image and the filter, the CGFH-based method can lead to an increase in the accuracy of optical data processing compared to the case of using SLM with a purely amplitude characteristic.

The use of devices with a hybrid amplitude–phase modulation for the implementation of the GFSF can lead to an increase in noise and distortion in the output plane of the optical system. An alternative method for implementing a Fourier filter in this case may be the optimal projection method. With bipolar amplitude modulation, the quadrature sub-pixel method with double resolution redundancy can be used to represent the complex values of the Fourier filter. An important feature of this method is the need to orient the SLM plane with respect to the direction of the read beam, which provides a phase difference of $\pi/2$ between the beams scattered by adjacent pixels.

Thus, the current state of the component base of spatial light modulation devices in combination with current methods for the synthesis of holographic elements make it possible to implement optical systems with a given complex impulse response function. This circumstance makes it possible to create devices for multi-channel parallel data processing and imaging with a resolution (number of channels) of up to 10^6 elements and an update frequency of up to 1 MHz.

Acknowledgements. The author is grateful to R.S. Starikov and S.B. Odinokov for useful discussions of the materials of this paper.

References

1. Miller D.A.B. *J. Lightwave Technol.*, **35** (3), 346 (2017).
2. Lin Shu-Feng, Kim Eun-Soo. *Opt. Express*, **25** (10), 11389 (2017).
3. Armitage D., Underwood I., Wu Shin-Tson. *Introduction to Microdisplays* (Chichester: John Wiley & Sons Ltd, 2006).
4. Cheremkhin P.A., Krasnov V.V., Rodin V.G., Starikov R.S. *Laser Phys. Let.*, **14** (2), 026202 (2017).
5. Chao Tien-Hsin, Hanan Jay, Zhou Hanying, Reyes George. *Proc. SPIE*, **5437**, 13 (2004).
6. Fukuchi Norihiro, Inoue Takashi, Toyoda Haruyoshi, Hara Tsutomu. *Chin. Opt. Let.*, **7** (12), 1131 (2009).
7. Evtikhiev N.N., Starikov S.N., Protsenko E.D., Zlokazov E.Yu., Solyakin I.V., Starikov R.S., Shapkarina E.A., Shaulskiy D.V. *Quantum Electron.*, **42**, 1039 (2012) [*Kvantovaya Elektron.*, **42**, 1039 (2012)].
8. Manzur T., Zeller J., Serati St. *Appl. Opt.*, **51** (21), 4976 (2012).
9. Monjur M.S., Tseng S., Tripathi R., Donoghue J.J., Shahriar M.S. *J. Opt. Soc. Am. A*, **31** (1), 41 (2013).
10. https://www.optalysys.com (2019).
11. Goodman J.W. *Introduction to Fourier Optics* (New York: McGraw-Hill, 1968; Moscow: Mir, 1970).
12. Vijaya Kumar B.V.K., Mahalanobis A., Juday R.D. *Correlation Pattern Recognition* (Cambridge, UK: Cambridge University Press, 2005).
13. Inoue Ayano, Usami Ren, Saito Keisuke, Honda Yasunobu, Ikeda Kanami, Watanabe Eriko *Tech. Dig. ISOM'18* (Kitakyushu, 2018) We-L-05.
14. Kasprzak H. *Appl. Opt.*, **21** (18), 3287 (1982).
15. Kasprzak H. *Appl. Opt.*, **40** (32), 5943 (2001).
16. Chang Julie, Sitzmann Vincent, Dun Xiong, Heidrich Wolfgang, Wetzstein Gordon. *Nat. Sci. Rep.*, **8**, 12324 (2018).
17. Kerekes R.A., Vijaya Kumar B.V.K. *Opt. Eng.*, **47** (6), 067202 (2008).
18. Evtikhiev N.N., Shaulskiy D.V., Zlokazov E.Yu., Starikov R.S. *Proc. SPIE*, **8398**, 83980G (2012).
19. Hornbeck L.J. Patent US5583688A (1996).
20. Bloom D.M. *Proc. IEEE Int. Electron Devices Meeting* (San Francisco, 1994).
21. Amm D.T., Corrigan R.W. *Proc. SPIE*, **3634**, 71 (1999).
22. De Bougrenet de la Tocnaye J.L., Dupont L. *Appl. Opt.*, **36** (8), 1730 (1997).
23. Goncharov D.S., Krasnov V.V., Ponomarev N.M., Starikov R.S. *Proc. SPIE*, **10558**, 105580Y (2018).
24. Goncharov D.S., Evtikhiev N.N., Krasnov V.V., Ponomarev N.M., Starikov R.S. *Comput. Opt.*, **43** (2), 200 (2019).
25. Bauchert K.A., Serati St.A., Sharp G.D., McKnight D.J. *Proc. SPIE*, **3073**, 170 (1997).
26. Birch Ph.M., Young R., Budgett D., Chatwin C. *Opt. Lett.*, **25** (14), 1013 (2000).
27. Jang Ju-Seog, Shin Dong-Hak. *Opt. Lett.*, **26** (22), 1797 (2001).
28. Domjan Laszlo, Koppa Pal, Szarvas Gabor, Remenyi Judit. *Optik*, **113** (9), 382 (2002).
29. Evtikhiev N.N., Zlokazov E.Yu., Krasnov V.V., Rodin V.G., Starikov R.S., Cheremkhin P.A. *Quantum Electron.*, **50**, 667 (2020) [*Kvantovaya Elektron.*, **50**, 667 (2020)].
30. Juday R.D., Florence J.M. *Proc. SPIE*, **1558**, 499 (1991).
31. Gregory D.A., Kirsch J.C., Tam E.C. *Appl. Opt.*, **31** (2), 163 (1992).
32. Neto Luiz Goncalves, Roberge Danny, Sheng Yunlong. *Appl. Opt.*, **35** (23), 4567 (1996).
33. Park Sungjae, Roh Jinyoung, Kim Soobin, Park Juseong, Kang Hoon, Hahn Joonku, Jeon Youngjin, Park Shinwoong, Kim Hwi.*Opt. Express*, **25** (4), 3469 (2017).
34. Cai Jianjun, Shen Xueju, Fan Cong, Kong Dezhao, Huang Fuyu. *Laser Phys. Lett.*, **16** (6), 066201 (2019).
35. Brown B.R., Lohmann A.W. *Appl. Opt.*, **5** (6), 967 (1966).
36. Brown B.R., Lohmann A.W. *IBM J. Res. Development*, **13** (2), 160 (1969).
37. Lohmann A.W., Paris D.P. *Appl. Opt.*, **6** (10), 1739 (1967).
38. Lohmann A.W., Paris D.P. *Appl. Opt.*, **7** (4), 651 (1968).
39. Lee Wai Hon. *Appl. Opt.*, **9** (3), 639 (1970).
40. Burckhardt C.B. *Appl. Opt.*, **9** (8), 1949 (1970).
41. Gabor D. *Nature*, **161**, 777 (1948).
42. Yaroslavsky L. *Introduction to Digital Holography* (Bentham E-books, 2009).
43. Cutrona L., Leith E., Palermo C., Porcello L. *IRE Trans. Inform. Theory*, **6** (3), 386 (1960).
44. Vander Lugt B.A. *IEEE Trans. Inform. Theory*, **IT-10**, 139 (1964).
45. Evtikhiev N.N., Starikov S.N., Sirotkin S.A., Starikov R.S., Zlokazov E.Yu. *Proc. SPIE*, **6977**, 69770C (2008).
46. Evtikhiev N.N., Starikov S.N., Zlokazov E.Yu., Sirotkin S.A., Starikov R.S. *Quantum Electron.*, **38**, 191 (2008) [*Kvantovaya Elektron.*, **38**, 191 (2008)].
47. Evtikhiev N.N., Shaulskiy D.V., Zlokazov E.Yu., Starikov R.S. *Proc. SPIE*, **8748**, 87480O (2013).
48. Shaulskiy D., Evtikhiev N., Starikov R., Starikov S., Zlokazov E. *Proc. SPIE*, **9094**, 90940K (2014).
49. Betin A.Yu., Bobrinev V.I., Odinokov S.B., Evtikhiev N.N., Starikov R.S., Starikov S.N., Zlokazov E.Yu., *Appl. Opt.*, **52** (33), 8142 (2013).
50. Betin A.Yu., Bobrinev V.I., Evtikhiev N.N., Zherdev A.Yu., Zlokazov E.Yu., Lushnikov D.S., Markin V.V., Odinokov S.B., Starikov S.N., Starikov R.S. *Quantum Electron.*, **43** (1), 87 (2013) [*Kvantovaya Elektron.*, **43** (1), 87 (2013)].
51. Betin A.Yu., Dontchenko S.S., Kovalev M.S., Odinokov S.B., Solomashenko A.B., Zlokazov E.Yu. *Tech. Dig. Digital Holography and 3D Imaging Meeting* (Shanghai, 2015) DW2A.20.
52. Horner J.L., Gianino P.D. *Appl. Opt.*, **23** (6), 812 (1984).
53. Gianino P.D., Horner J.L. *Opt. Eng.*, **23** (6), 695 (1984).
54. Gerchberg R.W., Saxton W.O. *Optik*, **35** (2), 1 (1972).
55. Yang Guo-zhen, Dong Bi-zhen, Gu Ben-yuan, Zhuang Jie-yao, Ersoy Okan K. *Appl. Opt.*, **33** (2), 209 (1994).
56. Dorsch R.G., Lohmann A.W., Sinzinger St. *Appl. Opt.*, **33** (5), 869 (1994).
57. Zalevsky Z., Mendlovic D., Dorsch R.G. *Opt. Lett.*, **21** (12), 842 (1996).

58. Hwang Hone-Ene, Chang Hsuan T., Lie Wen-Nung. *Opt. Lett.*, **34** (24), 3917 (2009).
59. Zlokazov E.Yu. *Japan. J. Appl. Phys.*, **58**, SKKD04 (2019).
60. Goncharov D.S., Zlokazov E.Yu., Petrova E.K., Ponomarev N.M., Starikov R.S. *Bull. Lebedev Phys. Inst.*, **46** (4), 126 (2019) [*Kr. Soobshch. Fiz. FIAN*, No. 4, 27 (2019)].
61. Hsueh C.K., Sawchuk A.A. *Appl. Opt.*, **17** (24), 3874 (1978).
62. Florence J.M., Juday R.D. *Proc. SPIE*, **1558**, 487 (1991).
63. Arrizon V., Sánchez-de-la-Llave D. *Appl. Opt.*, **41** (17), 3436 (2002).
64. Juday R.D. *Appl. Opt.*, **32** (26), 5100 (1993).
65. Laude V., Refregier Ph. *Appl. Opt.*, **33** (20), 4465 (1994).
66. Juday R.D. *J. Opt. Soc. Am. A*, **18** (8), 1882 (2001).
67. Birch Ph., Young R., Chatwin C., Farsari M., Budgett D., Richardson J. *Opt. Commun.*, **175**, 347 (2000).
68. Birch Ph., Young R., Budgett D., Chatwin C. *Opt. Lett.*, **26** (12), 920 (2001).
69. Birch Ph.M., Young R.C.D., Budgett D.M., Koukoulas Triantafillos, Li Gongde, Claret-Tournier F., Chatwin C.R. *Proc. SPIE*, **4089**, 393 (2000).
70. Van Putten E.G., Vellekoop I.M., Mosk A.P. *Appl. Opt.*, **47** (12), 2076 (2008).